Article

Not peer-reviewed version

New Insight into the Mechanism of Oxidative Degradation of Artistic White Acrylic Paint Based on Zinc Oxide: Uneven Distribution of Damage in the Paint Layer Under Artificial Aging Conditions

Mais Khadur , Victor Ivanov , Artem Gusenkov , Alexander Gulin , Marina Soloveva , Yulia Diakonova , Yulian Khalturin , Victor Nadtochenko *

Posted Date: 3 September 2025

doi: 10.20944/preprints202509.0383.v1

Keywords: acrylic artists' paint; polymer degradation; photocatalysis ZnO; photo-Kolbe reaction; ATR-FTIR spectroscopy; Raman spectroscopy-microscopy; chemometrics; PCA analysis

 doi:10.20944/preprints202509.0383.v1

Article

New Insight into the Mechanism of Oxidative Degradation of Artistic White Acrylic Paint Based on Zinc Oxide: Uneven Distribution of Damage in the Paint Layer Under Artificial Aging Conditions

Mais Khadur [1], Victor Ivanov [2], Artem Gusenkov [1,2], Alexander Gulin [1,2], Marina Soloveva [1], Yulia Diakonova [1,3], Yulian Khalturin [3] and Victor Nadtochenko [1,2,4,*]

[1] Moscow Center for Advanced Studies, Kulakova str. 20, Moscow, 123592, Russia.
[2] Federal Research Center for Chemical Physics RAS, Kosigin str. 4, 119991, Russia
[3] State Tretyakov Gallery, 10 Lavrushinsky Lane, Moscow, 119017 Russia.
[4] Chemical Department, Lomonosov Moscow State University, Leninskie Gory, 1, Moscow 119991, Russia
* Correspondence: nadtochenko@gmail.com

Abstract

Accelerated artificial aging of ZnO PW4 acrylic artist's paints was carried out for a total of 1963 hours (~8 10^7 lux.h) with aging assessment at specific intervals. Color change $\Delta E^* < 2$ (CIELab-76 system) over 1725 hours of aging, while the human eye notices color change at $\Delta E^* > 2$. Oxidative degradation of organic components in the paint to form volatile products was revealed by ATR-FTIR, Raman spectroscopy-microscopy and scanning electron microscopy with energy dispersive X-ray spectroscopy (SEM-EDS). It appears that deep oxidation of organic intermediates and volatilization of organic matter may be responsible for the relatively small value of ΔE^* color difference during aging of the samples. To elucidate the degradation pathways, principal component analysis (PCA) was applied to the spectral data, revealing: 1) the catalytic role of ZnO in accelerating photodegradation, 2) the Kolbe photoreaction, 3) the decomposition of the binder to form volatile degradation products, 4) the relative photoinactivity of $CaCO_3$ compared to ZnO, showing slower degradation in areas with higher $CaCO_3$ content compared to those dominated by ZnO. These results provide fundamental insights into formulation-specific degradation processes, offering practical guidance for the development of more durable artist paints and conservation strategies for acrylic artworks.

Keywords: acrylic artists' paint; polymer degradation; photocatalysis ZnO; photo-Kolbe reaction; ATR-FTIR spectroscopy; Raman spectroscopy-microscopy; chemometrics; PCA analysis

1. Introduction

Acrylic binder paint appeared on the American art market in the early 1950s under the commercial name "Magna" and immediately gained popularity among artists. The advertising slogan of the Bocour Artist Colors company, which produced the paint, presented the new product as "the first new painting technique in 500 years", which was essentially fair, given the two techniques that had dominated throughout the history of easel painting - oil-based and emulsion-based (tempera). [1] Painters quickly appreciated the advantages of the new product over traditional techniques, which consisted of the rapid drying of the paint, the intensity of color that was preserved even in the thinnest translucent layers, and the durability of the new product. Due to the high homogeneity of the paint mass, the new technique was well suited for creating large, uniform in color and texture painting planes, uniform in color, shine and texture, where the brushstroke was completely leveled. All these properties of paints gave artists new pictorial possibilities, and

 doi:10.20944/preprints202509.0383.v1

accordingly it can be said that the invention of acrylic had a direct and significant impact on artistic technique (in the understanding of not only the material, but also the direct creative work - the formation of an image, the creation of texture, the application of layers) and in general on the pictorial art of the second half of the twentieth century. The scale of the use of acrylic paints is evidenced, in particular, by the fact that the collection of the State Tretyakov Gallery in Russia contains about 500 works from the second half of the 20th century, executed in the technique of acrylic painting. As it turns out, acrylic paints can degrade over time, showing noticeable changes in color, gloss, and surface texture. [2–6]. This deterioration has been demonstrated through accelerated aging studies involving thermal and light-induced ageing[2,7–13]. Artists' acrylic emulsion paints contain various additives, such as coalescing agents, thickeners, defoamers, pH buffers, preservatives, surfactants, and wetting/dispersing agents, that influence performance properties[4–6]. These additives are designed to adsorb or chemically bond to pigment and extender surfaces to enhance dispersion stability, viscosity control, opacity, and durability [14]. However, environmental factors (UV exposure, heat, moisture, oxidation) can degrade destabilize these additives over time, altering the paint performance[4–6]. Accelerated aging studies have shown that degradation processes significantly enhance the migration of surfactants (polyethylene oxide (PEO)-based types, which predominate in acrylic emulsion formulations) from the base polymer matrix to the surface [3,7,15]. In particular, PEOs exhibit a tendency to oxidative degradation over time. [16,17]. To investigate acrylic paint degradation mechanisms, Attenuated Total Reflection Fourier Transformed Infrared (ATR-FTIR) and Raman spectroscopy are employed as powerful, rapid analytical techniques [8,18,19]. However, the interpretation of spectral data in acrylic paint aging studies presents a significant challenge due to the complexity and size of the data sets. [8,20]. Chemometric algorithms, particularly principal component analysis PCA [20,21] can be effective for investigating the aging of acrylic paints using ATR-IR and Raman spectroscopy.

The aim of this study is to investigate the aging of white acrylic ZnO-based artistic paints under artificial conditions: 1) checking color changes; 2) characterizing the evolution of the paint layer structure and assessing changes in the chemical composition of aged paint; 4) clarifying the mechanism of paint degradation. The acquired findings provide a comprehensive understanding of degradation processes in commercial ZnO acrylic artists' paint, demonstrating chemometrics (PCA) as an effective analytical methodology for spectral data analysis.

2. Materials and Methods

2.1. Samples Preparation

Commercial white acrylic artist's paint based on ZnO pigment P.W.4 was used. A uniform layer of ZnO-based white acrylic paint was applied to aluminum foil substrate using a medium brush, and then dried at ambient conditions (approximately 22 °C and 40% RH) for two weeks.

2.2. Artificial Daylight Ageing

The accelerated UV ageing of the paint samples conducted in Q-sun chamber under controlled conditions (38°C, 65% relative humidity RH). The radiation was produced by a Xe lamp simulating outdoor solar conditions (λ > 290 nm) with a radiation intensity of about 60 W/m^2. To study the kinetics of aging, individual probes of the sample were periodically taken. The maximum aging time in the chamber was 1963 hours, which, taking into account that for the spectrum of sunlight 685 Lux = 1 W/m^2, corresponds to 8.110^7 Lux·hour.

2.3. Colorimetric Measurements

Determination of colorimetric characteristics and reflectance spectra in the range of 400–700 nm was carried out on a ColorFlex spectrophotometer (HunterLab, USA) in the following mode: 45/0°,

 doi:10.20944/preprints202509.0383.v1

observation angle 10°, light source D65. The value of color difference ΔE in the CIELab-76 system was used as the main criterion. [22]

2.4. Scanning Electron Microscopy (SEM)

Electron microscopy images of aged samples were obtained using Prisma E (Thermo Fisher Scientific, Czech Republic). Samples intended for secondary electron imaging only were pre-coated with 40 nm layer of gold by Q150R ES plus sputter coater (Quorum Technologies, Great Britain) and additionally mounted by a copper tape for better charge drain. Chemical mapping and elemental analysis of aged samples was carried out using energy-dispersive X-ray spectroscopy (EDS) in a low vacuum mode.

2.5. Attenuated Total Reflection Fourier Transform Infrared Spectroscopy (ATR-FTIR)

The infrared spectra of the paint samples were acquired in attenuated total reflectance (ATR) mode using a Vertex -70 FTIR spectrometer (Bruker, Germany), Platinum Diamond ATR. Spectra were recorded in the range of 600–4000 cm^{-1} with a resolution of 4 cm^{-1}, averaging 64 scans per measurement. For each sample, ten ATR-FTIR measurements were collected from different randomly selected surface areas.

2.6. Raman Spectroscopy

For comprehensive chemical analysis and complete molecular fingerprint, Raman spectroscopy was used as a complementary technique to ATR-FTIR. Raman spectra were acquired using Raman microscope spectrometer Senterra (Bruker) equipped with a λ=785 nm excitation laser and a 50× objective with numerical aperture NA=0.75. The spatial resolution of microscope in measuring Raman spectra was estimated as 1.22* λ/NA≈1.3 μm. For each sample, 10 Raman spectra were collected from different randomly selected points on the sample surface.

2.7. ATR-FTIR, Raman Spectra Preprocessing

The obtained raw spectral data of ATR-FTIR and Raman scattering were pre-processed: smoothing, baseline correction, wavenumber range selection, normalization and analysis of outlier. Smoothing was performed using spectral filters removing random noise using the Savitzky-Golay (SG) algorithm.[23] An iterative polynomial fitting method was applied for the estimate of the baseline in Raman spectra.[24] The derivative treatment of data by the SG algorithm emphasize band widths, positions, and separations while simultaneously reducing or eliminating baseline and background effects. Differentiating data using the SG algorithm emphasizes the width of bands, positions, and splits while reducing or eliminating baseline and background effects.[25] The positions of the peaks of the ATR-FTIR spectra were determined by recording the minima of the second derivative of the ATR-FTIR spectra or, in the case of poorly separated bands, additionally by measuring the positions of the maxima of the fourth derivative of the same spectra. Principal component analysis (PCA) is a class of so-called unsupervised learning or pattern recognition methods. [26] In the present study, the purpose of using PCA was primarily to discover hidden structure, such as a pattern or grouping, in a dataset without prior knowledge of the pattern itself. Mean centering was performed in PCA [27]. PCA was also used to detect outliers.[28]

3. Results

3.1. Colometry

The results of color change due to samples aging are shown in Table 1. The results include the colorimetric changes in the values of the lightness/ darkness (L*), red/green (a*), yellow/blue (b*), and the total color change from 0 to 970 hours exposure (ΔE*). The color difference value ΔE in the CIELab-76 system used as the main criterion was determined using equation (1):

 doi:10.20944/preprints202509.0383.v1

$$\Delta E = [(\Delta L^*)^2 + (\Delta a^*)^2 + (\Delta b^*)^2]^{1/2} \quad (1)$$

where $\Delta L^* = L^*_i - L^*_0$, $\Delta a^* = a_i - a_0$, $\Delta b^* = b_i^* - b_0^*$, where index 0 refers to the sample before aging, and index i to the sample after a certain period of aging.

Table 1. Colorimetric characteristics of the aged layer of ZnO white acrylic paint PW4.

time, hours	L*	a*	b*	ΔE*
0	94.75	-1.29	4.04	0.77
120	95.06	-0.71	3.63	0.78
240	95.19	-0.7	3.78	0.75
360	95.17	-0.68	3.92	1.19
480	95.76	-0.66	4.14	1.18
730	95.72	-0.62	4.05	1.08
850	95.63	-0.69	4.22	1.08
970	95.61	-0.63	4.03	1.53
1090	95.81	-0.62	3.66	1.31
1240	94.96	-0.53	4.36	0.85
1360	95.56	-0.55	4.07	1.1
1480	95.60	-0.49	3.88	1.18
1600	95.64	-0.44	3.74	1.27
1725	95.56	-0.51	3.67	1.18

ΔE* value below 2 indicates a color difference that is barely perceptible to the average human observer. ΔE* must be >2 to be., while a ΔE* value greater than 2 becomes perceptible by the human eye. By comparing the colorimetric values of the white paint samples during 1725 hours of photoaging, we can realize that the ΔE* value is below 2. However, there is a slight increase in a* value (shifted to red). The rise in L* parameter suggests the increase in L* due to the changes in the surface roughness, as a rougher surface will scatter more light, increasing L*[29]. Also, the surfactant migration to the paint film surface can affect the gloss of this film [15] which in turn affect the L* values.

3.2. SEM Images

Figure 1 demonstrates SEM images of the sample before aging and samples aged for 1963 hours. Detailed changes in the SEM images of the paint layer at different aging times are shown in Figure SI1. (Supplementary Information). In the unaged sample, a uniform paint layer consisting of binder and pigment is observed (Figure 1A1, A2). After 1963 hours of aging (Figure 1B1, B2), significant microstructural changes were observed, including pronounced surface roughness and the appearance of pigment microcrystals zinc oxide (ZnO) and calcium carbonate ($CaCO_3$) [23]. The observed changes suggest the binder degradation. To reduce paint costs and increase its volume, $CaCO_3$ is commonly used as an extender, partially replacing ZnO [2]. While $CaCO_3$ influences paint stability, opacity, gloss, and film toughness, it indirectly influences acrylic binder deterioration[30,31]. $CaCO_3$ scatters and reflects UV radiation, reducing direct UV exposure and offering partial protection to the paint film[17]. Particle size analysis (Figure1,B1) further indicated that the $CaCO_3$ (calcite) grains ranged from 0.2 to 1 μm in size with the typical euhedral to subhedral habit[32], while ZnO particles (~100-200 nm) with hexagonal sectional shape (wurtzite crystal structure)[33].

 doi:10.20944/preprints202509.0383.v1

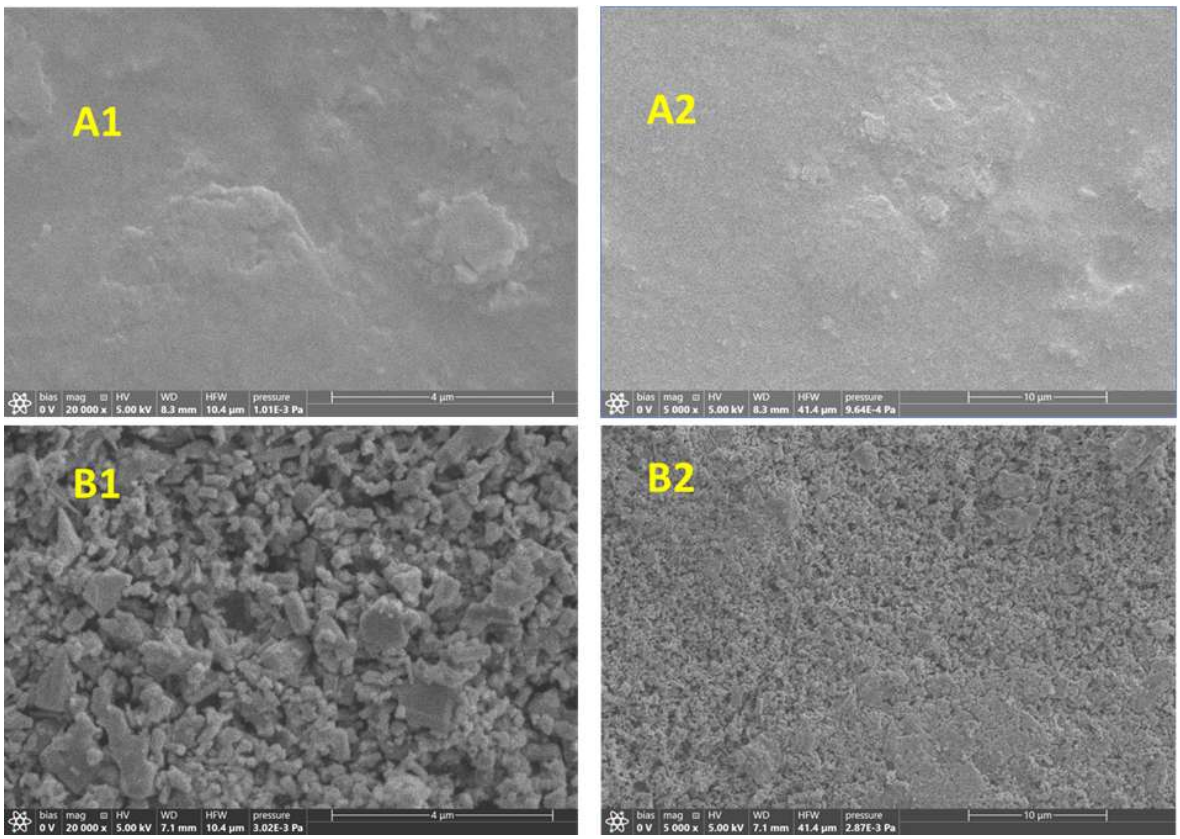

Figure 1. SEM images of the sample before aging (A1, scale bar 4 μm, A2, scale bar 10 μm) and samples aged for 1963 hours (B1, scale bar 4 μm, B2, scale bar 10 μm).

3.3. SEM-EDS Analysis of the Zinc White PW4 Acrylic Paint

The results of the SEM-EDS analysis of the zinc white PW4 acrylic paint are summarized in Figure 2, and the analysis details are presented in Figure SI2, Table SI1. In addition to carbon (C) and oxygen (O) peaks from the polymeric binder, zinc (Zn) peaks confirmed the ZnO as the primary pigment, while calcium (Ca) peaks corresponded with the $CaCO_3$ as an extender. SEM-EDS analysis shows significant differences in the distribution of ZnO and $CaCO_3$ nanocrystals in the dyed layer of the sample, as shown in Figure 2. Areas of the sample with elevated calcium content are clearly visible, shown in green in Figures 2B and 2D. The regions where zinc oxide dominates over $CaCO_3$ are clearly visible in Figures 2C and 2D (red dots). The approximate size of the region of increased $CaCO_3$ concentration is from ~3 to ~15 μm. Apparently, such heterogeneity of the sample layer can be manifested when measuring spectra on a Raman microscope with a resolution of about 1.3 μm and, possibly, when measuring ATR-FTIR spectra (see below).

 doi:10.20944/preprints202509.0383.v1

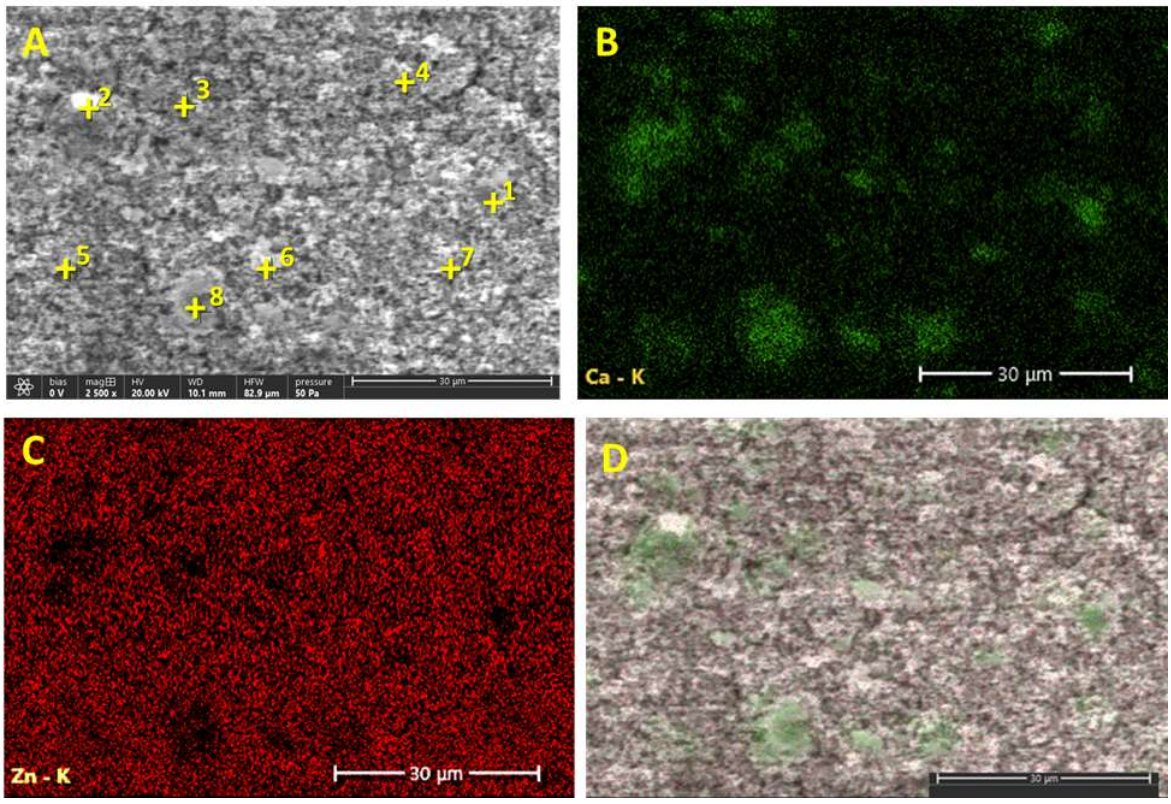

Figure 2. SEM-EDS images of the sample stained with acrylic paint PW4. A. SEM image, points indicate areas of EDS analysis (the analysis results are documented in SI 2). B. SEM-EDS image of calcium distribution in the stained sample. C. SEM-EDS image of zinc distribution in the stained sample. D. Superimposed SEM-EDS/SEM image, zinc (red) and calcium (green).

The SEM-EDS results of paint samples indicated spatial heterogeneity in elemental distribution across the paint surface (SI2). While most areas showed strong ZnO predominance ($ZnO/CaCO_3$ > 20:1), isolated regions revealed near-equivalent ZnO and $CaCO_3$ content (~1:1 ratio) indicating $CaCO_3$ agglomeration. This indicates that the surfactant and dispersant system used in the paint formulation do not provide a sufficiently uniform distribution of ZnO and $CaCO_3$. Trace of elements (Si, S, and K <1 wt%) was detected in localized regions likely due to incidental impurities or residual processing additives.

3.4. Aging of Acryl Zinc White PW4 Paint Revealed by ATR-FTIR Spectroscopy

Figure 3 manifests the main motif of changes in the ATR-FTIR averaged spectra of a zinc white layer during aging using a fresh and aged 1963-hour sample as an example. In the ATR-FTIR spectrum of the fresh sample, the bands of the organic components of the paint dominate, whereas in the aged sample, the bands of the organic component are inferior in intensity to the band of the inorganic components, in particular $CaCO_3$. Figure 3 and Figure SI3 (the detailed evolution of average spectra during aging) depicts a pronounced degradation of the acrylic component peak at 1727 cm^{-1}.The intensity of the CO_3^{2-} peaks associated with $CaCO_3$, in particular the peak of 876 cm^{-1}, increases relative to peaks of the organic component. These changes suggest the degradation of organic components of the paint. The acquired ATR-FTIR spectra of the unaged paint sample (summarized in Table 2) were dominated bands of the acrylic binder. The stretching vibrations of carbonyl ether groups C=O were observed at 1727 cm^{-1}, the stretching vibrations of the C–H bond at (2873, 2930 and 2956 cm−1) and the vibrations of ether groups (–C–C(=O)–O–) at (1159 and 1254 cm^{-1}) can be tentative attributed to acrylic chains. The bands corresponding to =C–H stretching (at 3083,

 doi:10.20944/preprints202509.0383.v1

3061, and 3027 cm^{-1}), C=C aromatic stretching (at 1603 and 1493 cm^{-1}), and C–H bending (at 759 and 698 cm^{-1}) obtained due to ν(C=C) bending and out-of-plane C–H bending (759 and 698 cm^{-1}) suggest the presence of a styrene-acrylic copolymer blend as a binder. The stretching vibrations of C-O-C groups (at 1102, 1118, 992, and 1060 cm^{-1}) were ascribed to a non-ionic surfactant polyethylene oxides (PEO) [3]. Weak bands at 1414, 874, and 712 cm^{-1} indicated the presence of calcium carbonate ($CaCO_3$) [34]. A broad, weak band at 1563 cm^{-1} assigned to asymmetric stretching vibrations of COO^- groups, suggested the presence of a poly(acrylic acid) (PAA) used likely as a dispersant, likely forming metal–carboxylate complexes with the extender and pigment particles [3,35,36]. PAA shows also characteristic peaks of ester groups as acrylic chain. Additionally, a weak shoulder at 1670 cm^{-1}, assigned to the hydrogen-bonded C=O stretching vibration from the interactions between residual carboxylic acid (-COOH) groups and binder carbonyl (C=O) groups.

Table 2. Characteristic ATR-FTIR bands in white acrylic artists' paint PW 4. A tentative assignment of peaks was made based on the analysis of the spectra in the form of second or fourth derivatives.

ATR-FTIR (cm-1) the present study	**IR absorption band (cm^{-1})**	**Functional group assignment**	**Compound assignment**
31130-3600	3130-3600	–OH associated stretching vibration	PAA, Aging products, Water, and H-bonded[2,37]
3027, 3044, 3060, 3086	3027-3059-3085	=C-H stretch (aromatic)	Polystyrene [20,25]
2927, 2959,	2956 -2930-	$–CH_2$ and –CH3 asymmetric stretching vibration	Polyethylene oxides (PEO) non-ionic surfactant PAA, Acrylic medium[3,38,39]
2853, 2868	2873, 2856	–CH2, -CH3 symmetric stretching vibrations	Polyethylene oxides (PEO)non-ionic surfactant, Acrylic medium, PAA[3,38,39]
1727	1725	–C=O stretching vibration	Acrylic medium[3]
1675, 1686, 1699	1675	–C=O (H-bonded) stretching vibration	Acrylic medium , PAA [40]
1624, 1637	1632	C=C stretching	Aging product[11,41–43]
1603	1600		Polystyrene [7,44]
1596 - 1624	1600 to1636	O–H bending vibration	Adsorbed water[3,45]
1560, 1576	1562	COO^- asymmetric stretching (carboxylate)	Metal carboxylate complexes[35,36]
1487, 1500, 1516	1492	Aromatic C=C in-plane bending, C–C ring stretching.[7]	Polystyrene [37,38,44,46]

 doi:10.20944/preprints202509.0383.v1

1448, 1458	1452	-CH2 bending vibrations	Polystyrene [44], PAA, Acrylic medium [3,39,47,48]
1414	1414	CO_3^{2-} stretching vibration (ν3)	Calcium carbonate extender [3,34,49–51]
1371, 1387, 1401	1395-1300	–CH3 , –CH2 Bending vibration	Polyethylene oxides (PEO) non-ionic surfactant ,Acrylic medium[3]
1156, 1180, 1206, 1222, 1244, 1266	1267, 1254, 1159	C-O stretching vibration	PAA, Acrylic medium [15]
1095, 1110, 1122	1118, 1102	–C–O–C– stretching vibration	Polyethylene oxides (PEO) non-ionic surfactant [3,7]
1026, 1066	1027-1064	-C–O- stretching vibration	PAA, Acrylic medium [38]
902,912,922,940,963	906-940-963	C-H out-of-plane bending vibration	Polystyrene [38,52]
876	874	CO_3^{2-} stretching vibration (ν_2)	Calcium carbonate extender[8,53]
843	846	C_H rocking vibration	Acrylic medium, Polystyrene [42,44]
712	712	CO_3^{2-} stretching vibration (ν_4)	Calcium carbonate extender[8,53]
701	700, 732, 760	C–H bending vibration	Acrylic medium [7,8], Polystyrene[44]

The use of averaged spectra Figure 3 is due to the fact that the spectra obtained from different points of the sample differ somewhat (see Figure SI4). The deviation of spectra measured from different random points relative to the average spectrum increases in the region of organic compound bands as the sample ages, which is not observed for bands of inorganic compounds, such as $CaCO_3$. These deviations in the spectra of the aged sample are apparently due to the uneven distribution of the paint components ZnO and $CaCO_3$, revealed by SEM (Figure 2), as well as different degradation rates in different areas of the sample.

 doi:10.20944/preprints202509.0383.v1

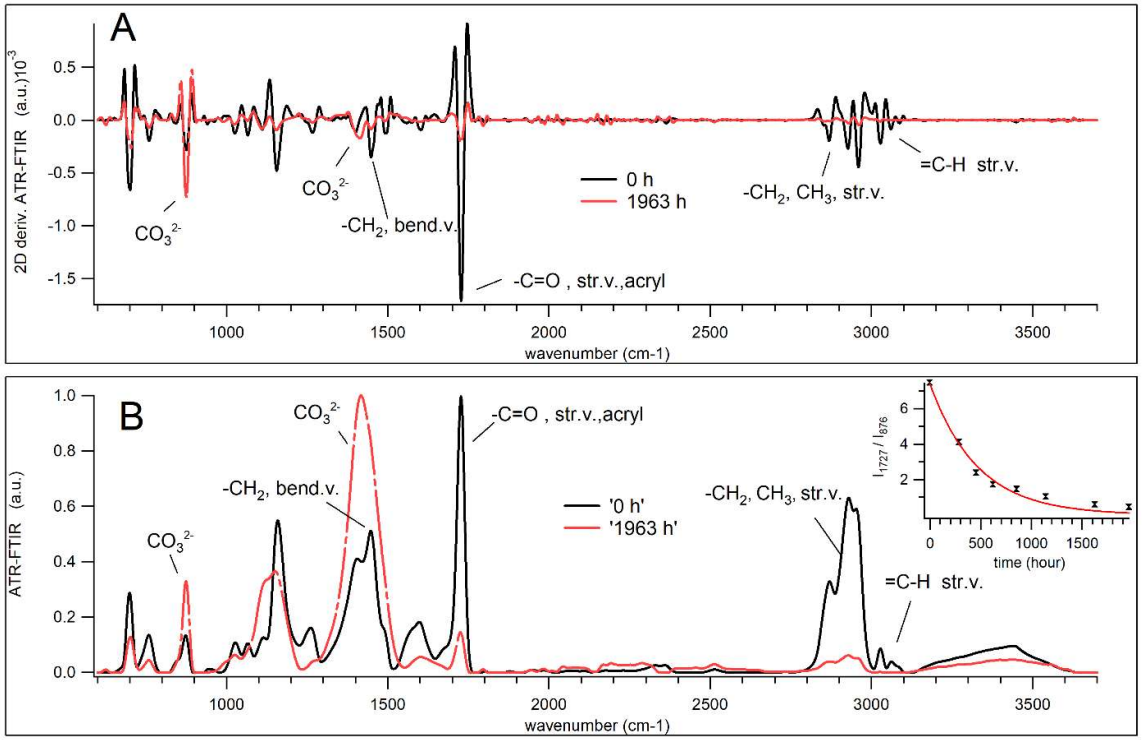

Figure 3. ATR-FTIR average spectra of the nonaged 0 hour and aged 1963-hour acrylic zinc white PW4 samples. The averaged spectra were obtained from ten spectra measured at random points on the sample. Spectra are normalized to the minimum-maximum scale (SI1). A, ATR-FTIR spectra in the form of second derivatives. B, averaged ATR-FTIR spectra. Insert, kinetics of decay of the I_{1727}/I_{876} ratio, exponential fit with rate constant 0.00213 ± 0.00016 1/hour.

It can be assumed that the concentration of CaCO3 during the aging process of the sample is almost constant, since chemically inert inorganic CaCO3 is stable compared to the organic components of the paint. Therefore, to quantitatively characterize the kinetics of degradation of an organic binder, the ratio of the acrylate band intensity to the $CaCO_3$ band intensity I_{1727}/I_{876} can be used as a marker. The ratio of the intensity of the C-H band to the $CaCO_3$ band (I_{2928}/I_{876} and I_{3027}/I_{876}) can also be used as an additional marker. Figure 4 shows the averaged FTIR spectra normalized to the peak intensity at 876 cm^{-1}. In this representation, Figure 4 manifests the kinetics of all markers I_{1727}/I_{876}, I_{2928}/I_{876} and I_{3027}/I_{876}. The exponential fit predicts a characteristic degradation time of 469 hour for the acrylic component of 1727 cm^{-1} (insert Figure 3B). The decay time is equal to 287 hours for the band of 2928 cm^{-1} and 271 hours for the band of 3027 cm^{-1}.

 doi:10.20944/preprints202509.0383.v1

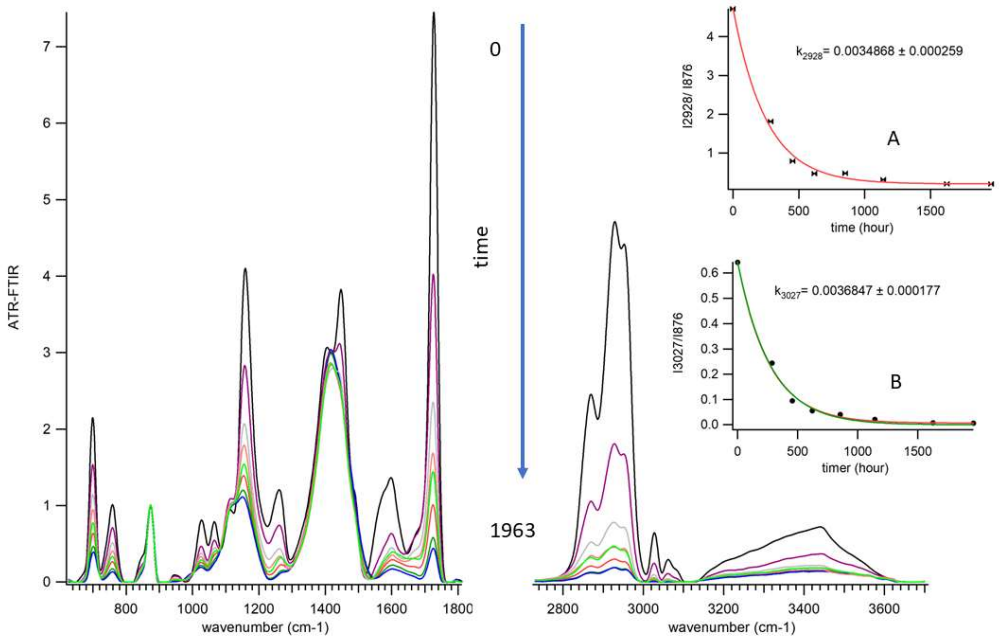

Figure 4. ATR-FTIR average spectra at aging time of 0, 287, 455, 621, 855, 1143, 1626, and 1963 hours. Spectra are normalized to the peak at 876 cm^{-1}(SI3.2). Insert A, experimental points of kinetics I_{2928}/I_{876}. Solid line is exponential fit exp(-k·time), k=0.0035 1/hour. Insert B, experimental points of kinetics I_{3027}/I_{876}. Solid line is exponential fit exp(-k·time), k=0.0037 1/hour.

3.5. Aging of Acryl Zinc White PW4 Paint Revealed by Raman Spectroscopy-Microscopy

Due to the high spatial resolution Raman microscopy (~1.3 μm) and the complex composition of the paint with non-uniform distribution of paint components in the layer (see Figure 2), the Raman spectra measured from different points of the same sample turned out to be variable (see Figure SI5). This fact apparently indicates a different rate of degradation of the binder at different points of the sample (see Figure SI5). The averaged spectra for all points measured in the sample and their derivatives were analyzed to determine the positions of the Raman band peaks (Figure SI6). Raman peaks are summarized in Table 3. Raman spectra of the samples (Table 3) revealed characteristic peaks corresponding to the vibrational modes of ZnO, which confirms the presence of ZnO as a pigment in the wurtzite phase. The most intense peak at 438 cm^{-1} was attributed to the E_2(high) mode, the shoulder at 328 cm^{-1} was attributed to second-order scattering (E_2), a very weak shoulder around 384 cm^{-1} corresponded to the A_1(TO) mode, and a weak peak at 546 cm^{-1} was associated with defective ZnO or probably originated from impurities [54,55]. Additionally, overlapping peaks in the region (700 -900 cm^{-1}) were attributed to vibrations in acrylic binder, PEO and polystyrene. A strong peak appeared at 1006 cm^{-1} accompanied by a shoulder at 1033 cm^{-1}, corresponded to aromatic ring vibrations in styrene. The peaks at 284, 712, and 1086 cm^{-1} were associated with $CaCO_3$[53,56,57]. These findings are consistent with the ATR-FTIR results.

Table 3. Raman peak assignments for ZnO acrylic paint film before and after 1963 hours of simulated daylight exposure.

	Raman shift (cm^{-1})	**Functional group assignment**	**Compound assignment**
1086	1086	Symmetric CO_3^{2-} Stretch (ν_1)	Calcium carbonate extender[53,56,57]

 doi:10.20944/preprints202509.0383.v1

1034	1038	C-H in-plane bending (aromatic ring)	Polystyrene [58]
999	1000	C-H symmetric in-plane vibrations (aromatic ring)	Polystyrene[20,38,58]
752,799,843	700-900	Vibrations of C-O, –C–COO, C-O-C, C-C and= C-H groups	Polystyrene, Polyethylene oxides (PEO) non-ionic surfactant (PEO), Acrylic medium [59]
708	712	In-plane CO_3^{2-}Bend (ν_4)	Calcium carbonate extender[53,56,57]
619	612, 760	C-H out-of-plane bending (aromatic ring)	Polystyrene [38,58,60]
543	546	A_1(LO) phonon mode (defective ZnO)	Zinc Oxide pigment[55,61]
433	438	E_2(high) mode	Zinc Oxide pigment[54,55]
380	384	A_1(TO) mode	Zinc Oxide pigment[54,55]
332	328	E_2(low) mode	Zinc Oxide pigment[54]

Raman method is effective in detecting the ZnO peaks and aromatic ring changes corresponding to polystyrene. It is reasonable to assume that zinc oxide is not destroyed during the aging process of the sample. Based on this assumption, the peak intensity ratio I_{999}/I_{876} can be used as a marker for quantitative characterization of the aromatic ring degradation kinetics. The averaged Raman spectra normalized to the 433 cm^{-1} peak associated with ZnO (SI3.2) corresponding to different aging times are shown in Figure 5. The kinetics of the decay of the aromatic ring at 999 cm^{-1} is shown in the inset to Figure 5. The rate constant of aromatic ring decay estimated as an exponential fit is ~0.001 1/hour. This is ~3.5 times slower than the C-H decay estimate made from the ATR-IR data (Figure 4). It can be assumed that such a difference in the degradation rate of different organic groups is due to their different localization relative to the ZnO crystals (see below).

 doi:10.20944/preprints202509.0383.v1

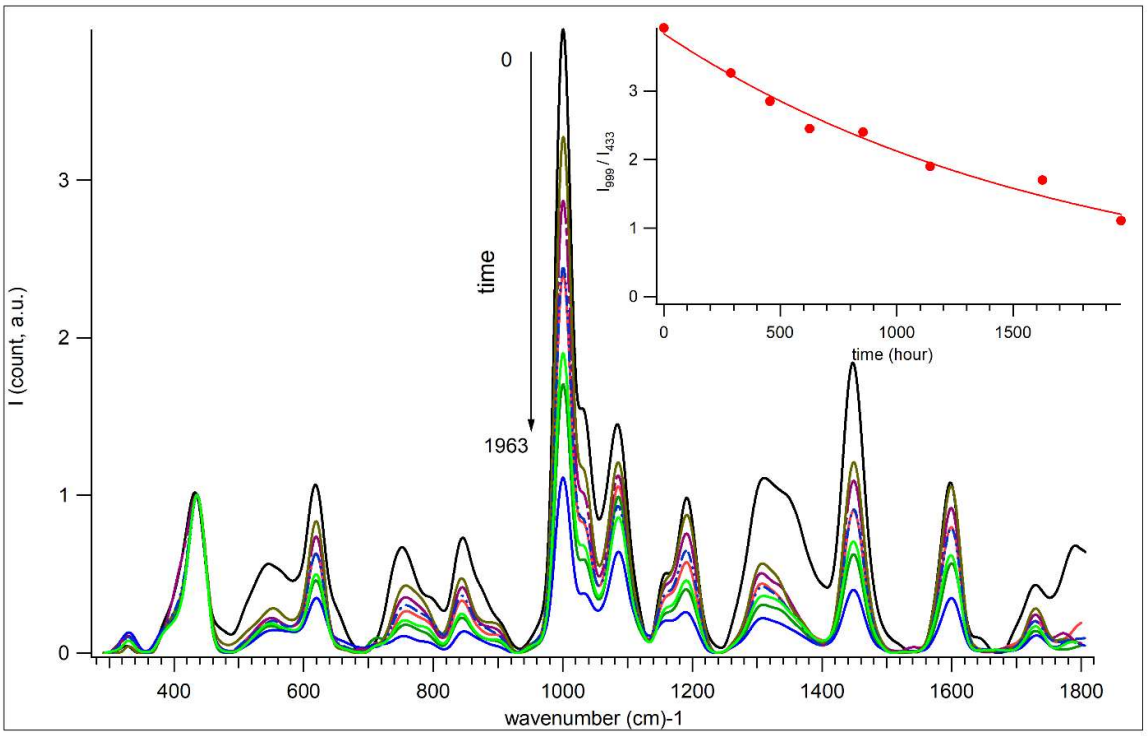

Figure 5. Raman spectra of PW4 acrylic paint samples at different aging times. Scaling: all average spectra are normalized to the peak of 433 cm^{-1} associated with ZnO. Inset A shows the decay of the peak of 999 cm^{-1} over time.

Spectral variations that exist between different points of the same sample may be due to different rates of sample degradation or other uncontrolled experimental factor. All this makes the interpretation of Raman and ATR-FTIR spectra difficult without the use of chemometrics, which has become indispensable for eliminating confounding effects and extracting subtle spectral variations of interest from the measured spectra (see below).

3.6. PCA Analysis of ATR-FTIR Spectra

PCA analysis was performed separately on the ATR spectra in the ranges (600–1850 cm^{-1}) and (2700-3700 cm^{-1}), considering all samples over the aging period. The scores plots (PC1 vs. PC2) for both spectral ranges (Figure 6) displayed distinct sample clustering by aging time, confirming progressive degradation.

 doi:10.20944/preprints202509.0383.v1

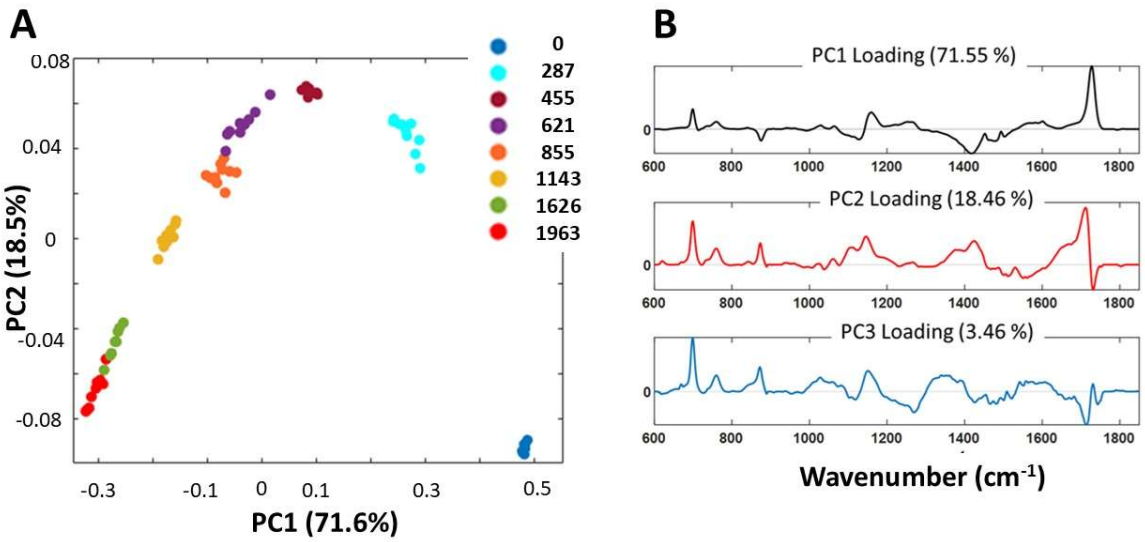

Figure 6. PCA Analysis results of ATR-FTIR Spectra in the range (600–1850 cm^{-1}). Vector normalization was used (SI3.3). A. PC2 vs PC1 scores. B. PC1, PC2 and PC3 loadings.

In the Spectral Range (600–1850 cm^{-1})

Principal component 1 (PC1, 71.5% variance) captured the dominant photodegradation trends in total (Figure 6A). Where, the positive loadings (representing decreasing peaks intensities) revealed decreases in:

a) C–O stretching vibrations (at 1027, 1060, 1159, 1254, and 1267 cm^{-1}) and carbonyl C=O stretching (at 1725 cm^{-1}), indicating the degradation of the acrylic chains.

b) Characteristic polystyrene vibrations (at 700, 732, 760, and 1604 cm^{-1}) and out-of-plane deformations (906-940, 963 cm^{-1}), confirming the polystyrene degradation.

c) COO^- stretching (at 1562 cm^{-1}), suggesting disruption of metal-carboxylate complex.

d) C=O (H-bonded) stretching vibration (at 1675, shoulder) attributed to the degradation of the dispersant PAA and further degradation of degradation products.

Conversely, negative peaks (representing increasing intensities) showed: a) $CaCO_3$ bands (at 712, 874 and 1414 cm^{-1}), as well as a broadening at (1527–1307 cm^{-1}), reflecting a relative increase in the intensity of the $CaCO_3$ band as a result of the degradation of the binder and dispersant (PAA); b) increased C-O-C stretching (at 992, 1102, and 1118 cm^{-1}), consistent with the surfactant PEO migration to the film surface.

PC2 (18.46 % variance) elucidated initial chemical changes in the paint film during the light exposure period (287 - 455 hours). The spectra after 455 hours of exposure exhibited the highest positive value in the PC2 scores plot, indicating most advanced degradation state in this period. The PC2 loading highlighted the following spectral changes:

a) Asymmetric broadening of the carbonyl peak (at 1725 cm^{-1}) toward lower wavenumbers (~1710 cm^{-1}), indicating the formation of new C=O species from oxidative degradation of the PAA, acrylic , and styrene chains[7];

b) Narrowing of the carbonyl ester peak on the higher wavenumber side, consistent with oxidative cleavage ester groups in the acrylic binder;

c) Increase in the shoulder intensity at 1675 cm^{-1}, due to change in hydrogen-bonding induced shifts in carbonyl (C=O) stretching frequencies, providing additional evidence for the formation of new C=O groups;

 doi:10.20944/preprints202509.0383.v1

d) Broadening of the $CaCO_3$ absorption band (1414cm-1) especially, near 1427 cm^{-1} and 1370 cm^{-1}), due to the binder degradation and $CaCO_3$ exposure;

e) Broadening of C-O-C stretching bands (at the peak 1102cm^{-1} and shoulder 1118 cm^{-1}) reflecting the migration and reorganization of the surfactant (PEO);

f) Decreased intensity at ~1620, consistent with the loss of the adsorbed water[3,45].

PC3 (3.46% Variance) tracked intermediate aging changes in the paint film, where the spectra acquired after 621 hours of light exposure showed the highest positive value in the PC3 scores plot (Figure SI8, SI9). The corresponding PC3 loading plot (Figure 6B) revealed narrowing of the ester carbonyl peak, accompanied by a reduction in the (H-bonded C=O) band at 1675 cm^{-1}, suggesting a decline in carboxylic acid (–COOH) groups due to further degradation;

3.7. In the Spectral Range (2700–3700 cm^{-1})

PC1 (78.29% Variance) represented the dominant degradation pattern, with positive loadings corresponding to a decrease in peak intensity for:

a) Stretching vibrations of CH_3 and CH_2 (at 2868, 2927, and 2959 cm^{-1}) and =C–H (3027, 3044, 3060, 3086 cm^{-1}), indicating the breakdown and degradation of the (acrylic-styrene) binder chains;

b) The broad IR band (3130–3600 cm^{-1}), attributed to O–H groups, suggesting weakened H-bonding between PEO and paint components, and initial water desorption at the beginning of the aging, and the formation of volatile products as aging advances.

PC2 (12.3 % variance) reflected the significant baseline variations during the aging process. In the PC2 scores plot (Figure 7A), the sample aged for 455 hours showed the highest value, confirming the early-stage transformations detected by PC2 in the 600–1850 cm^{-1} range. The corresponding loadings plot (Figure 7B) highlighted the transient changes including:

a) Asymmetric broadening of C-H stretching vibrations band (at~ 2700-2850 cm^{-1}), likely corresponds to the formation of the degradation products e.g., aldehyde 2695-2830 cm^{-1} (weak Fermi doublet at 2720, 2820 cm^{-1} that are registered for aged samples);

b) Non-uniform reduction in peak intensity, where the PC2 positive loadings represented the spectral regions which were more resistant to decrease, such as (symmetric stretching vibrations at 2873cm^{-1}). In contrast, negative loadings represented bands more susceptible to radical attack, including asymmetric stretching vibrations of the –C–H groups of alkenes and aromatic compounds.

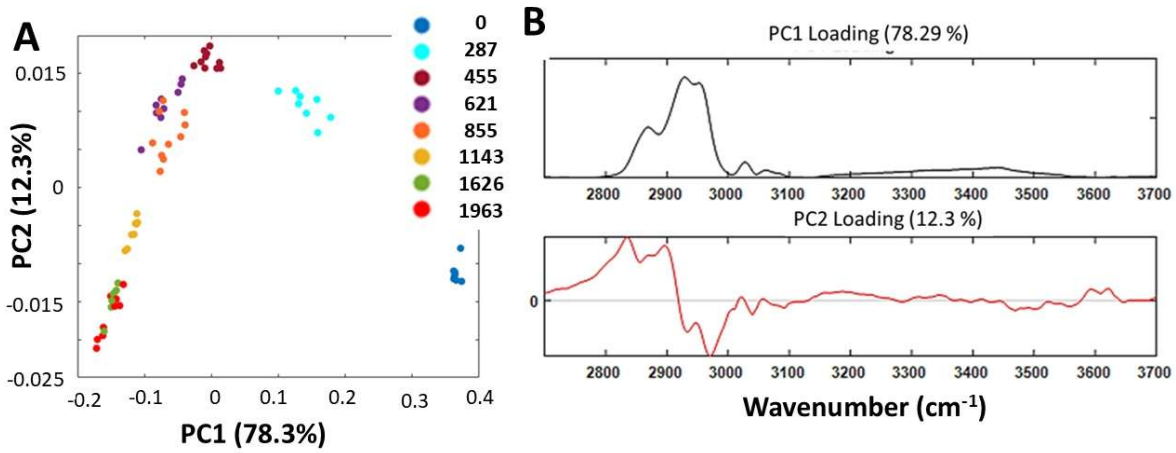

 doi:10.20944/preprints202509.0383.v1

Figure 7. PCA analysis results of ATR-FTIR spectra in the range (2700–3700 cm^{-1}). Vector normalization was used (SI3.3). A. PC2 vs PC1 scores. B. PC1, PC2 and PC3 loadings.

3.8. PCA Analysis of Raman Spectra

Raman technique is particularly more effective for detecting the changes of ZnO and aromatic ring (PS), owing to its high sensitivity to these characteristic molecular vibrations. In this study, PCA was applied to the spectral range of 150–1130 cm^{-1} and which 300-1800 cm^{-1} covers key vibrational modes of ZnO, PS, $CaCO_3$, and C=O groups. Due to the high spatial resolution Raman spectroscopy-microscopy (spot size ~1.3 μm) and the complex distribution of ZnO and $CaCO_3$ in the paint layer (Figure 2), the Raman spectra were quite variable, as mentioned above. Before mean centering, two Raman spectral scaling procedures were used for PCA analysis: vector normalization was applied to the spectral range 150–1130 cm^{-1} and normalization was applied to the intensity of the ZnO peak at 433 cm^{-1} to the spectral window of 300-1800 cm^{-1}. Scaling according to vector normalization leads to greater scattering in the score plot (see SI7. PCA analysis of Raman spectra). Figure 8 shows a plot of the scores and loadings when the spectra are normalized to the ZnO peak at 433 cm^{-1}. The score plot (Figure 8) shows trends in PC1(82.6%) and PC2 (10.46%) changes with aging time similar to those observed PC1 and PC2 of the ATR-FTIR spectra (Figure 6 and 7). At the same time, PCA analysis of Raman spectra shows a wider spread of PC1, PC2 scores associated with each specific aged sample, compared to similar scores for ATR-FTIR spectroscopy. The high spatial resolution of Raman microscopy makes it possible to detect areas with different rates of degradation of the organic binder, i.e., areas with a high ZnO content and areas with an increased $CaCO_3$ content. For example, in Fig. SI 13e, SI 14 show that the Raman spectra of the sample aged for 1963 hours can be divided into two groups of similar spectra, which can apparently be attributed to the region of fast and slow degradation of the polymer binder. This observation, together with the SEM-EDS data confirming the non-uniform dispersion of the filler with high ZnO or $CaCO_3$ content, indicates localized heterogeneous degradation of organics.

 doi:10.20944/preprints202509.0383.v1

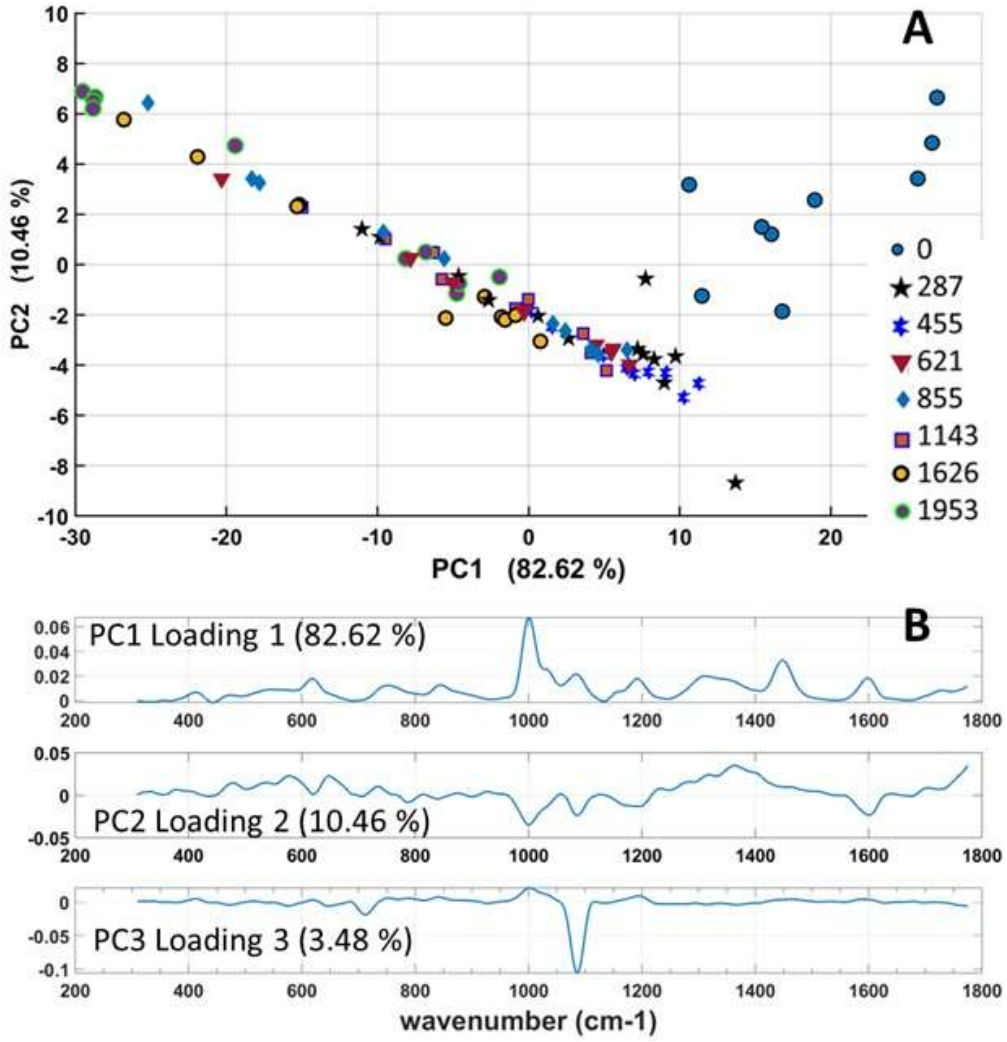

Figure 8. PCA Analysis results of Raman spectra in the range (300–1800 cm^{-1}). A. PC2 vs PC1 scores. B. PC1, PC2 and PC3 loadings.

The spectrum of PS1 Loading 1 (82.6 %) is similar in shape to the spectrum of the organic component of the paint (Figure 8B). This suggests that changes in the PC1 scores during sample aging are associated with organic degradation. The spectrum of PC2 Loading 2 (10.5%) shows that the change in PC2 during sample aging is associated with peaks at ~1000 cm^{-1} related to the aromatic ring, 1086 cm^{-1} $CaCO_3$, 1600 cm^{-1} C=O and a broad band consisting of several overlapping bands between 1230 cm^{-1} and 1450 cm^{-1}, which can be tentatively attributed to various carbon-carbon and carbon-hydrogen bonds. The spectrum of PC3 Loading 3 (~3.5%) reveals the peak of 1086 cm-1 $CaCO_3$. This suggests that the changes in the PC3 score correspond to an increase in the $CaCO_3$ peak intensity relative to the organic matter peaks during sample aging.

4. Discussion

4.1. Degradation Mechanism of Acrylic Paint ZnO PW4

The main degradation characteristics of ZnO PW4 paint can be summarized as follows: a) ATR-FTIR and Raman spectroscopy studies show that the degradation of ZnO PW4 acrylic paint is associated with the oxidation of the organic binder; b) SEM reveals deep oxidation with the formation

 doi:10.20944/preprints202509.0383.v1

of volatile low molecular weight products. Apparently, deep oxidation of organic semi-products and volatilization of organics may be the reason for the relatively small value of color difference ΔE during aging of samples; c) Raman spectroscopy-microscopy and ATR-FTIR spectroscopy display the uneven degradation of organic substances in the paint layer.

It is known that the presence of oxygen, light and heat leads to the degradation of polymers.[62] Chain radical reactions can be initiated in primary photochemical reactions followed by the autoxidation process (Scheme 1). Peroxy ($O_2^{\bullet-}$), hydroperoxy $HO_2^{\bullet}$ radical and peroxyl radicals $RO_2^{\bullet}$ are far more stable than either $HO^{\bullet}$ radical or the carbon-centered radical $R^{\bullet}$ and the related alkoxyl radicals $RO^{\bullet}$. The simplified Scheme 1 does not emphasize that the peroxyl radical $ROO^{\bullet}$ is a low-reactivity radical and reaction (11) may be kinetically thermodynamically disfavored for most organic components in polymer [62]. Thus, the deep and uneven oxidation of organic matter in ZnO paint is difficult to explain based solely on photochemically initiated autoxidation.

Photocatalytic reactions involving inorganic substances should be taken into account. $CaCO_3$ are wide band gap materials. The indirect energy gap is estimated to be 5.07 eV (245 nm) and the direct allowed optical transitions along high symmetry directions in the Brillouin zone give the fundamental absorption edge of ~6.0 eV (207 nm)[63] . As a result, $CaCO_3$ is photochemically inert in aging experiments. ZnO is a direct bandgap semiconductor with a bandgap energy E_g of ~3.2-3.4 eV[64]. It absorbs light in the ultraviolet (UV) range, approximately below a wavelength of ~385 nm. The flat band potential of ZnO ECB is around -0.46 to -0.88 eV vs. NHE (Normal Hydrogen Electrode). The EVB is the highest energy level in the valence band. It can be calculated using the formula: EVB = ECB + Eg ~ 2.3 eV. The electron and hole can act as highly reactive agents. [64] Lipovsky et al. reported that ZnO nanoparticles induce increased formation of reactive oxygen species, namely hydroxyl radicals and singlet oxygen, not only under UV light, but a remarkable enhancement of the oxy radicals was also found under visible light (400–500 nm). [65]

Scheme 1

Photocatalytic reactions

$ZnO + h\nu \rightarrow e^-_{cb} + h^+_{vb}$ (1)

$(O_2)_{ads} + e^-_{cb} \rightarrow O_2^{\bullet-} + H^+ \leftrightarrow HO_2^{\bullet}$ (2)

$h^+_{vb} + (H_2O \leftrightarrow H^+ + OH^-)_{ads} \rightarrow H^+ + HO^{\bullet}$ (3)

ZnO induced photo-Kolbe reaction

$R\text{-}COO^- + h^+(ZnO) \rightarrow R^{\bullet} + CO_2\uparrow$ (4)

Norrish type I mechanism (α-cleavage).

$R_1\text{–}C(=O)\text{–}OR' + h\nu \rightarrow R_1^{\bullet} + {}^{\bullet}C(=O)\text{–}OR'$ (5)

$R''H + {}^{\bullet}C(=O)\text{–}OR' \rightarrow R''^{\bullet}$ + Volatile Organic Compounds (VOC)+ CO_2 (6)

Autooxidation

$HO^{\bullet} + RH \rightarrow R^{\bullet} + H_2O$ (7)

$RO^{\bullet} + R'H \rightarrow ROH + R'^{\bullet}$ (8)

$R^{\bullet} \rightarrow \beta$-scission $\rightarrow R'^{\bullet}$ + low molecular weight products (9)

$R^{\bullet} + O_2 \rightarrow RO_2^{\bullet}$ (10)

$RO_2^{\bullet} + R'H \rightarrow ROOH + R'^{\bullet}$ (11)

$HO_2^{\bullet} + RH \rightarrow R^{\bullet} + H_2O_2$ (12)

$2RO_2^{\bullet} \rightarrow$ inactive products (13)

$RO_2^{\bullet} + R^{\bullet} \rightarrow ROOR$ (14)

$R^{\bullet} + R^{\bullet} \rightarrow R\text{-}R$ (15)

$ROOH \rightarrow RO^{\bullet} + HO^{\bullet}$ (16)

$R\text{-}O\text{-}O\text{-}R \rightarrow RO^{\bullet} + RO^{\bullet}$ (17)

$2ROOH \rightarrow RO_2^{\bullet} + RO^{\bullet} + H_2O$ (18)

$RO_2^{\bullet}$, $RO^{\bullet} \rightarrow$ (carboxylic acid, aldehyde, ketone, and vinyl groups…)

 doi:10.20944/preprints202509.0383.v1

Since ZnO is photocatalytically active and $CaCO_3$ is not, the oxidation of the organic components in the region of high $CaCO_3$ concentration is slower than in the region of enhanced ZnO concentration, where active radicals and oxygen species can be formed. This is probably the main reason for the uneven degradation rate of the organic binder.

PCA analysis of the ATR and Raman spectra showed that the degradation mechanism of acrylic paint ZnO has clearly defined stages associated with the formation of intermediate products of organic oxidation. For example, the accumulation of carboxyl compounds leads to the formation of radicals due to photo-Kolbe reaction (4) with the formation of R• radicals [66,67]. Due to the reduction in the content of ester bonds revealed by ATR-FTIR, it can be assumed that in parallel with the photocatalytic process, an important degradation pathway may occur through the oxidation of the C=O ester group, leading to cleavage at the α-carbon via the reactions (5), (6) of Norrish type I mechanism (α-cleavage) . This side chain scission mechanism generates two radical intermediates: (1) an α-carbon ester radical (•COOR') that undergoes hydrogen abstraction from another organic molecule, forming volatile fragments, and (2) a new centered radical [36,43,68,69].

The PC3 of ATR-FTIR spectra revealed the dominant chemical changes **occurring** at the aging intervals (621 and 855 hours), indicating an advanced stage of degradation. **The narrowing in C=O peak, along with the decline of the hydrogen-bonded C=O peak and the OH peak, suggested the oxidation of -COOH groups forming low-molecular-weight degradation products** [70]. **The progressive decrease in ester C=O and aromatic ring peaks intensities without emergence of new carbonyl shoulders confirmed that the binder degradation mechanism primarily involved the formation of volatile fragments.**

The final aging intervals (1143–1963 hours) and was primarily represented by PC1 analysis of the ATR-FTIR, Raman data, reflecting the complete degradation pathway . The PC1 loadings (Figure 6,8) revealed the key changes after 1963 hours of aging compared to the unaged paint. Here, the progressive decline in the aromatic ring content, the reduction in (bonded/ non-bonded) carbonyl bands, and the absence of the C=C peak indicated more severe stage of binder degradation driven by oxidation and volatile loss [7]. Consistent with the SEM observations, no significant crosslinking between the binder chains was detected, since the IR bands of (C-O-C) assosited to PEO did not show shift or emergence of new shoulder in this rigion. The continued decrease in the ATR-FTIR and Raman characteristic binder signals with the aging, further demonstrated that the primary degradation mechanisms were chain scission and volatile loss. On the other hand, PC1 and PC2 of the Raman data revealed significant spectra discrimination at this stage due to heterogeneous degradation, reflecting extreme degradation of the organic binder in ZnO-rich regions (Figure SI 13e)

5. Conclusion

The color change caused by aging of ZnO white PW4 was measured by the color difference value ΔE^* in the CIELab-76 system. The colorimetric values ΔE^* value is below 2 the during 1725 hours of sample aging (~7 10^7 Lux.h). It is generally accepted that the human eye notices a change in color when $\Delta E^*>2$. At the same time, SEM, ATR-FTIR and Raman spectroscopy show significant changes in the structure and chemical composition of the ZnO PW4 white paint layer during ~1000-1963 hours of aging. SEM showed increased surface roughness, cavitation, and chalkiness with the progressive degradation of the binder. The SEM results indicate deep oxidation with the formation of volatile low-molecular products. Apparently, deep oxidation of organic semi-products and volatilization of organics may be the reason for the relatively small value of the color difference ΔE during aging of the samples.

Raman spectroscopy microscopy and, to some extent, ATR -FTIR spectroscopy revealed uneven degradation of organic components on the surface of the paint layer. Analysis of spectral data using the principal component PCA method showed that the degradation of organic components of the paint occurs through the mechanism of chain radical oxidation with the initiation of the reaction as a result of the photocatalytic oxidation on ZnO microparticles. The uneven distribution of ZnO and $CaCO_3$ in the paint layer has been demonstrated at a micro scale by SEM-EDS. Carboxyl compounds

 doi:10.20944/preprints202509.0383.v1

present in paint or accumulated during oxidation of organic components can also serve as a source of active radicals due to the photo-Kolbe reaction. PCA of Raman data confirmed the photocatalytic role of ZnO in binder degradation, showing higher degradation rates in ZnO-rich regions compared to areas dominated by $CaCO_3$.

This study demonstrated the effectiveness of principal component analysis (PCA) in analyzing complex data sets related to the degradation kinetics of acrylic art paints and can provide guidance for the development of more durable ZnO-based acrylic paints. Importantly, since ZnO-based paint is highly susceptible to photoinduced degradation, the results highlight the need for careful selection of additives, particularly dispersants and surfactants. In this study, it was shown that dispersant (PAA) decarboxylation induced by ZnO photo-Kolbe reaction accelerates active radicals generation and binder degradation. In addition, the surfactant-dispersant system plays an important role in optimal dispersion of the filler in the paint matrix, thereby avoiding differences in degradation rates throughout the paint film.

Supplementary Materials: The following supporting information can be downloaded at the website of this paper posted on Preprints.org, SI1, Figure SI1: SEM images of the ZnO-based white acrylic artists' paint SEM images. SI2, Figure SI2: SEM image of the sample after 1963-hour aging; Table SI1: The relative content of elements at the points shown in Figure SI2. SI3, equation SI3.1: Scaling and normalization of spectra; equation SI3.2: Scaling and normalization of spectra. SI4, Figure SI3: ATR-IR spectra of acrylic zinc white paint PW4 during aging at time points of 0, 287, 455, 621, 855, 1143, 1626 and 1963 hours; Figure SI4: ATR-FTIR spectra of acrylic zinc white PW4 samples at different aging time. SI5, Figure SI5: Raman spectra of acrylic zinc white PW4 samples at different aging time; Figure SI6: Raman spectra of acrylic zinc white paint PW4 during aging at time points of 0, 287, 455, 621, 855, 1143, 1626 and 1963 hours in the form of the 2d derivative. SI6, Figure SI7: 3D plot of PC1, PC2 and PC3 scores of ATR-FTIR spectra in the range of 600–1850 cm^{-1}; Figure SI8: PC1 vs PC3 scores of ATR-FTIR spectra in the range of 600–1850 cm^{-1}; Figure SI9: PC2 vs PC3 scores of ATR-FTIR spectra in the range of 600–1850 cm^{-1}; Figure SI 10: 3D plot of PC1, PC2 and PC3 scores of ATR-FTIR spectra in the range of 2700–3700 cm^{-1}; Figure SI 11: PC1 vs. PC2 scores of ATR-FTIR spectra in the range of 2700–3700 cm^{-1}; Figure SI 12: PC1 vs. PC3 scores of ATR-FTIR spectra in the range of 2700–3700 cm^{-1}; Figure SI 12: PC1, PC2 and PC3 loadings of ATR-FTIR spectra in the range of 2700–3700 cm^{-1}. SI 7, Figure SI 13: PC1, PC2 and PC3 scores and loadings of Raman spectra: Figure SI 14: Hierarchical cluster analysis of the 1963-hour sample spectra.

Author Contributions: Investigation, formal analysis, methodology, writing—original draft preparation, Mais Khadur, resources, formal analysis Victor Ivanov, resources, data curation Artem Gusenkov, resources, data curation Alexandr Gulin, funding Marina Solovyeva, methodology, writing—original draft preparation Yulia Diakonova, methodology, writing—original draft preparation Yulian Khalturin, conceptualization, methodology, formal analysis, supervision, funding acquisition, writing—review and editing Victor Nadtochenko

Funding: This research was funded by the Russian Science Foundation,
grant #25-78-20011.

Data Availability Statement: Data will be available on request.

Acknowledgments: The experiments were carried out using the equipment of the Center for Collective Use of the Federal Research Center for Chemical Physics of the Russian Academy of Sciences "Analysis of Chemical-Biological Systems and Natural Materials".

Conflicts of Interest: The authors declare no conflicts of interest.

Abbreviations

 doi:10.20944/preprints202509.0383.v1

The following abbreviations are used in this manuscript:

MDPI	Multidisciplinary Digital Publishing Institute
DOAJ	Directory of open access journals
ATR-FTIR	Attenuated Total Reflectance Fourier-Transform Infrared spectroscopy
SEM	Scanning electron microscopy
SEM-EDS	Scanning electron microscopy with energy dispersive X-ray spectroscopy
PEO	Polyethylene oxide
VIS	Visible
UV	Ultraviolet
PCA	Principal component analysis
RH	Relative humidity
SG	Savitzky-Golay algorithm

References

1. Jablonski, E.; Learner, T.; Hayes, J.; Golden, M. Conservation Concerns for Acrylic Emulsion Paints. *Stud. Conserv.* **2003**, *48*, 3–12, doi:10.1179/sic.2003.48.supplement-1.3.
2. Alonso-Villar, E.M.; Rivas, T.; Pozo-Antonio, J.S. Resistance to Artificial Daylight of Paints Used in Urban Artworks. Influence of Paint Composition and Substrate. *Prog. Org. Coatings* **2021**, *154*, 106180, doi:10.1016/j.porgcoat.2021.106180.
3. Doménech-Carbó, M.T.; Silva, M.F.; Aura-Castro, E.; Fuster-López, L.; Kröner, S.; Martínez-Bazán, M.L.; Más-Barberá, X.; Mecklenburg, M.F.; Osete-Cortina, L.; Doménech, A.; et al. Study of Behaviour on Simulated Daylight Ageing of Artists' Acrylic and Poly(Vinyl Acetate) Paint Films. In Proceedings of the Analytical and Bioanalytical Chemistry; March 2011; Vol. 399, pp. 2921–2937.
4. Hagan, E.W.S.; Charalambides, M.N.; Young, C.R.T.; Learner, T.J.S. The Effects of Strain Rate and Temperature on Commercial Acrylic Artist Paints Aged One Year to Decades. *Appl. Phys. A Mater. Sci. Process.* **2015**, *121*, 823–835, doi:10.1007/s00339-015-9423-6.
5. Learner, T.; Chiantore, O.; Scalarone, D. Ageing Studies of Acrylic Emulsion Paints. *13th Trienn. Meet. ICOM CC Rio Janiero Prepr.* **2002**, 911–919.
6. Learner, T. A Review of Synthetic Binding Media in Twentieth-century Paints. *Conserv.* **2000**, *24*, 96–103, doi:10.1080/01410096.2000.9995156.
7. Pagnin, L.; Calvini, R.; Sterflinger, K.; Izzo, F.C. Data Fusion Approach to Simultaneously Evaluate the Degradation Process Caused by Ozone and Humidity on Modern Paint Materials. *Polymers (Basel).* **2022**, *14*, doi:10.3390/polym14091787.
8. Hamidi, F.; Aslani, F. Tio2-Based Photocatalytic Cementitious Composites: Materials, Properties, Influential Parameters, and Assessment Techniques. *Nanomaterials* **2019**, *9*, doi:10.3390/nano9101444.
9. Whitmore, P.M.; Colaluca, V.G. The Natural and Accelerated Aging of an Acrylic Artists' Medium. *Stud. Conserv.* **1995**, *40*, 51–64, doi:10.1179/sic.1995.40.1.51.
10. Nguyen, T.V.; Dao, P.H.; Duong, K.L.; Duong, Q.H.; Vu, Q.T.; Nguyen, A.H.; Mac, V.P.; Le, T.L. Effect of R-TiO2 and ZnO Nanoparticles on the UV-Shielding Efficiency of Water-Borne Acrylic Coating. *Prog. Org. Coatings* **2017**, *110*, 114–121, doi:10.1016/j.porgcoat.2017.02.017.
11. Nguyen, T.V.; Dao, P.H.; Nguyen, T.A.; Dang, V.H.; Ha, M.N.; Nguyen, T.T.T.; Vu, Q.T.; Nguyen, N.L.; Dang, T.C.; Nguyen-Tri, P.; et al. Photocatalytic Degradation and Heat Reflectance Recovery of Waterborne Acrylic Polymer/ZnO Nanocomposite Coating. *J. Appl. Polym. Sci.* **2020**, *137*, doi:10.1002/app.49116.
12. Dodd, A.C.; McKinley, A.J.; Saunders, M.; Tsuzuki, T. Effect of Particle Size on the Photocatalytic Activity of Nanoparticulate Zinc Oxide. *J. Nanoparticle Res.* **2006**, *8*, 43–51, doi:10.1007/s11051-005-5131-z.
13. Garcia-Segura, S.; Brillas, E. Applied Photoelectrocatalysis on the Degradation of Organic Pollutants in Wastewaters. *J. Photochem. Photobiol. C Photochem. Rev.* **2017**, *31*, 1–35, doi:10.1016/j.jphotochemrev.2017.01.005.
14. Vu, T.V.; Nguyen, T.V.; Tabish, M.; Ibrahim, S.; Huong, T.; Hoang, T.; Gupta, R.K.; My, T.; Dang, L.; Nguyen, T.A.; et al. Water-Borne ZnO/Acrylic Nanocoating: Fabrication, Characterization, and Properties. **2021**, 1–10.

 doi:10.20944/preprints202509.0383.v1

15. Digney-Peer, S.; Burnstock, A.; Learner, T.; Khanjian, H.; Hoogland, F.; Boon, J. The Migration of Surfactants in Acrylic Emulsion Paint Films. *Stud. Conserv.* **2004**, *49*, 202–207, doi:10.1179/sic.2004.49.s2.044.
16. Anghelone, M.; Jembrih-Simbürger, D.; Pintus, V.; Schreiner, M. Photostability and Influence of Phthalocyanine Pigments on the Photodegradation of Acrylic Paints under Accelerated Solar Radiation. *Polym. Degrad. Stab.* **2017**, *146*, 13–23, doi:10.1016/j.polymdegradstab.2017.09.013.
17. Tao, Y.; Mao, Z.; Yang, Z.; Zhang, J. CaCO3 as a New Member of High Solar-Reflective Filler on the Cooling Property in Polymer Composites. *J. Vinyl Addit. Technol.* **2021**, *27*, 275–287, doi:10.1002/vnl.21801.
18. Joseph, E.; Ricci, C.; Kazarian, S.G.; Mazzeo, R.; Prati, S.; Ioele, M. Macro-ATR-FT-IR Spectroscopic Imaging Analysis of Paint Cross-Sections. *Vib. Spectrosc.* **2010**, *53*, 274–278, doi:10.1016/j.vibspec.2010.04.006.
19. Gomes De Oliveira, A.G.; Wiercigroch, E.; De Andrade Gomes, J.; Malek, K. Infrared and Raman Spectroscopy of Automotive Paints for Forensic Identification of Natural Weathering. *Anal. Methods* **2018**, *10*, 1203–1212, doi:10.1039/c7ay02684f.
20. Mokari, A.; Guo, S.; Bocklitz, T. Exploring the Steps of Infrared (IR) Spectral Analysis: Pre-Processing, (Classical) Data Modelling, and Deep Learning. *Molecules* **2023**, *28*, 1–21, doi:10.3390/molecules28196886.
21. Pagnin, L.; Calvini, R.; Wiesinger, R.; Weber, J.; Schreiner, M. Photodegradation Kinetics of Alkyd Paints: The Influence of Varying Amounts of Inorganic Pigments on the Stability of the Synthetic Binder. *Front. Mater.* **2020**, *7*, 1–15, doi:10.3389/fmats.2020.600887.
22. Mokrzycki, W.S.; Tatol, M. Color Difference Delta E - A Survey. *Mach. Graph. Vis.* **2012**, *20*, 383–411.
23. Bromba, M.U.A.; Ziegler, H. Application Hints for Savitzky-Golay Digital Smoothing Filters. *Anal. Chem.* **1981**, *53*, 1583–1586, doi:10.1021/AC00234A011.
24. Liland, K.H.; Kohler, A.; Afseth, N.K. Model-Based Pre-Processing in Raman Spectroscopy of Biological Samples. *J. Raman Spectrosc.* **2016**, *47*, 643–650, doi:10.1002/jrs.4886.
25. Rinnan, Å.; Berg, F. van den; Engelsen, S.B. Review of the Most Common Pre-Processing Techniques for near-Infrared Spectra. *TrAC Trends Anal. Chem.* **2009**, *28*, 1201–1222, doi:10.1016/J.TRAC.2009.07.007.
26. Coccato, A.; Caggiani, M.C. An Overview of Principal Components Analysis Approaches in Raman Studies of Cultural Heritage Materials. *J. Raman Spectrosc.* 2024, *55*, 125–147. doi:10.1002/jrs.6621
27. Kim, D.; You, K. PCA, SVD, and Centering of Data. **2023**. *arXiv preprint arXiv:2307.15213*.
28. Mujica, L.E.; Rodellar, J.; Fernández, A.; Güemes, A. Q-Statistic and T2-Statistic Pca-Based Measures for Damage Assessment in Structures. *Struct. Heal. Monit.* **2011**, *10*, 539–553, doi:10.1177/1475921710388972.
29. Whitmore, P.M.; Colaluca, V.G. The Natural and Accelerated Aging of an Acrylic Artists' Medium. *Stud. Conserv.* **1995**, *40*, 51–64, doi:10.1179/sic.1995.40.1.51.
30. Senler, S.; Eren, M.; Mert, S. Progress in Organic Coatings Effect of Wollastonite Extender on the Properties of Exterior Acrylic Paints. **2016**, *93*, 34–40, doi:10.1016/j.porgcoat.2015.12.014.
31. Alvarez, V.; Paulis, M. Effect of Acrylic Binder Type and Calcium Carbonate Filler Amount on the Properties of Paint-like Blends. *Prog. Org. Coatings* **2017**, *112*, 210–218, doi:10.1016/j.porgcoat.2017.07.023.
32. Ševčík, R.; Šašek, P.; Viani, A. Physical and Nanomechanical Properties of the Synthetic Anhydrous Crystalline CaCO3 Polymorphs: Vaterite, Aragonite and Calcite. *J. Mater. Sci.* **2018**, *53*, 4022–4033, doi:10.1007/s10853-017-1884-x.
33. Manabeng, M.; Mwankemwa, B.S.; Ocaya, R.O.; Motaung, T.E.; Malevu, T.D. A Review of the Impact of Zinc Oxide Nanostructure Morphology on Perovskite Solar Cell Performance. *Processes* **2022**, *10*, 1–19, doi:10.3390/pr10091803.
34. Cai, G. Bin; Chen, S.F.; Liu, L.; Jiang, J.; Yao, H. Bin; Xu, A.W.; Yu, S.H. 1,3-Diamino-2-Hydroxypropane-N,N,N′,N′-Tetraacetic Acid Stabilized Amorphous Calcium Carbonate: Nucleation, Transformation and Crystal Growth. *CrystEngComm* **2010**, *12*, 234–241, doi:10.1039/b911426m.
35. Zhang, Y.; Gard, T.; Theron, C.; Apostoluk, A.; Masenelli-Varlot, K.; Canut, B.; Daniele, S.; Masenelli, B. Visible Luminescence Improvement of ZnO/PAA Nano-Hybrids by Silica Coating. *Appl. Surf. Sci.* **2021**, *540*, 148343, doi:10.1016/j.apsusc.2020.148343.
36. Yousif, E.; El-Hiti, G.A.; Haddad, R.; Balakit, A.A. Photochemical Stability and Photostabilizing Efficiency of Poly(Methyl Methacrylate) Based on 2-(6-Methoxynaphthalen-2-Yl)Propanoate Metal Ion Complexes. *Polymers (Basel).* **2015**, *7*, 1005–1019, doi:10.3390/polym7061005.

 doi:10.20944/preprints202509.0383.v1

37. Bosi, A.; Ciccola, A.; Serafini, I.; Guiso, M.; Ripanti, F.; Postorino, P.; Curini, R.; Bianco, A. Street Art Graffiti: Discovering Their Composition and Alteration by FTIR and Micro-Raman Spectroscopy. *Spectrochim. Acta - Part A Mol. Biomol. Spectrosc.* **2020**, *225*, doi:10.1016/j.saa.2019.117474.
38. Yabagi, J.A.; Kimpa, M.I.; Muhammad, M.N.; Rashid, S. Bin; Zaidi, E.; Agam, M.A. The Effect of Gamma Irradiation on Chemical, Morphology and Optical Properties of Polystyrene Nanosphere at Various Exposure Time. *IOP Conf. Ser. Mater. Sci. Eng.* **2018**, *298*, doi:10.1088/1757-899X/298/1/012004.
39. Zamo, A.; Rond, C.; Hamdan, A. Polystyrene (PS) Degradation Induced by Nanosecond Electric Discharge in Air in Contact with PS/Water. *Plasma* **2024**, *7*, 49–63, doi:10.3390/plasma7010004.
40. Wu, S.; Luo, Y.; Ran, Q.; Shen, J. Effects of Comb Copolymer PAA-g-MPEO on Rheological and Dispersion Properties of Aqueous CaCO3 Suspensions. *Polym. Bull.* **2007**, *59*, 363–370, doi:10.1007/s00289-007-0768-7.
41. Melo, M.J.; Bracci, S.; Camaiti, M.; Chiantore, O.; Piacenti, F. Photodegradation of Acrylic Resins Used in the Conservation of Stone. *Polym. Degrad. Stab.* **1999**, *66*, 23–30, doi:10.1016/S0141-3910(99)00048-8.
42. Beigzadeh, A.M.; Vaziri, M.R.R. Z-Scan Dosimetry of Gamma-Irradiated PMMA. *Nucl. Instruments Methods Phys. Res. Sect. A Accel. Spectrometers, Detect. Assoc. Equip.* **2021**, *991*, 165022, doi:10.1016/j.nima.2021.165022.
43. Wochnowski, C.; Metev, S.; Sepold, G. UV-Laser-Assisted Modification of the Optical Properties of Polymethylmethacrylate. *Appl. Surf. Sci.* **2000**, *154*, 706–711, doi:10.1016/S0169-4332(99)00435-3.
44. Yousif, E.; Haddad, R. Photodegradation and Photostabilization of Polymers, Especially Polystyrene: Review. *Springerplus* **2013**, *2*, 1–32, doi:10.1186/2193-1801-2-398.
45. Xu, J.J.; Lu, Y.N.; Tao, F.F.; Liang, P.F.; Zhang, P.A. ZnO Nanoparticles Modified by Carbon Quantum Dots for the Photocatalytic Removal of Synthetic Pigment Pollutants. *ACS Omega* **2023**, *8*, 7845–7857, doi:10.1021/acsomega.2c07591.
46. Budlayan, M.L.M.; Patricio, J.N.; Lagare-Oracion, J.P.; Arco, S.D.; Alguno, A.C.; Basilio, A.; Latayada, F.S.; Capangpangan, R.Y. Improvised Centrifugal Spinning for the Production of Polystyrene Microfibers from Waste Expanded Polystyrene Foam and Its Potential Application for Oil Adsorption. *J. Eng. Appl. Sci.* **2021**, *68*, 1–11, doi:10.1186/s44147-021-00030-y.
47. Pasichnyk, M.; Václavíková, M.; Gaálová, J.; Melnyk, I. Functional Finishing of Polyester Fabric With Polystyrene-Acrylic/Zno Nanocomposite for Effective Dyes Filtration. **2021**.
48. Bandyopadhyay, A.; Basak, G.C. Studies on Photocatalytic Degradation of Polystyrene. *Mater. Sci. Technol.* **2007**, *23*, 307–314, doi:10.1179/174328407X158640.
49. Rodriguez-Blanco, J.D.; Shaw, S.; Benning, L.G. The Kinetics and Mechanisms of Amorphous Calcium Carbonate (ACC) Crystallization to Calcite, via Vaterite. *Nanoscale* **2011**, *3*, 265–271, doi:10.1039/c0nr00589d.
50. Zhang, Z.; Xie, Y.; Xu, X.; Pan, H.; Tang, R. Transformation of Amorphous Calcium Carbonate into Aragonite. *J. Cryst. Growth* **2012**, *343*, 62–67, doi:10.1016/j.jcrysgro.2012.01.025.
51. Oriols, N.; Salvadó, N.; Pradell, T.; Butí, S. Amorphous Calcium Carbonate (ACC) in Fresco Mural Paintings. *Microchem. J.* **2020**, *154*, doi:10.1016/j.microc.2019.104567.
52. Dinoop lal, S.; Sunil Jose, T.; Rajesh, C.; Anju Rose Puthukkara, P.; Savitha Unnikrishnan, K.; Arun, K.J. Accelerated Photodegradation of Polystyrene by TiO2-Polyaniline Photocatalyst under UV Radiation. *Eur. Polym. J.* **2021**, *153*, 110493, doi:10.1016/j.eurpolymj.2021.110493.
53. Kim, Y.; Caumon, M.C.; Barres, O.; Sall, A.; Cauzid, J. Identification and Composition of Carbonate Minerals of the Calcite Structure by Raman and Infrared Spectroscopies Using Portable Devices. *Spectrochim. Acta - Part A Mol. Biomol. Spectrosc.* **2021**, *261*, 119980, doi:10.1016/j.saa.2021.119980.
54. Li, C.; Lv, J.; Zhou, B.; Liang, Z. Influence of Annealing Atmosphere on Optical Properties of Al-Doped ZnO Powders. *Phys. Status Solidi Appl. Mater. Sci.* **2012**, *209*, 1538–1542, doi:10.1002/pssa.201228004.
55. Bognár, S.; Jovanović, D.; Despotović, V.; Jakšić, S.; Panić, S.; Milanović, M.; Finčur, N.; Putnik, P.; Šojić Merkulov, D. Advanced Photocatalytic Degradation of Organic Pollutants Using Green Tea-Based ZnO Nanomaterials Under Simulated Solar Irradiation in Agri-Food Wastewater. *Foods* **2025**, *14*, 1–20, doi:10.3390/foods14040622.
56. Barroso-Solares, S.; Mediavilla-Martinez, I.; Sanz-Velasco, C.; Prieto, A.C.; Pinto, J. Pigments Identification and Analysis of the State of Conservation of the Decorative Elements of the Castle of Coca (XV-XVI AC, Segovia, Spain) by Raman Spectroscopy. *J. Phys. Conf. Ser.* **2022**, *2204*, doi:10.1088/1742-6596/2204/1/012010.

 doi:10.20944/preprints202509.0383.v1

57. Donnelly, F.C.; Purcell-Milton, F.; Framont, V.; Cleary, O.; Dunne, P.W.; Gun'ko, Y.K. Synthesis of CaCO3 Nano- and Micro-Particles by Dry Ice Carbonation. *Chem. Commun.* **2017**, *53*, 6657–6660, doi:10.1039/c7cc01420a.
58. Fan, Y.; Cornelius, C.J. Raman Spectroscopic and Gas Transport Study of a Pentablock Ionomer Complexed with Metal Ions and Its Relationship to Physical Properties. *J. Mater. Sci.* **2013**, *48*, 1153–1161, doi:10.1007/s10853-012-6853-9.
59. Bertoldo Menezes, D.; Reyer, A.; Benisek, A.; Dachs, E.; Pruner, C.; Musso, M. *Raman Spectroscopic Insights into the Glass Transition of Poly(Methyl Methacrylate)*; 2021; Vol. 23; ISBN 0000000175.
60. Boyden, M.N.; Kleist, E.M.; Asztalos, C.K.; Korter, T.M. Determination of the Polymer Composition of Mid-Twentieth Century Purses by Raman Spectroscopy. *Herit. Sci.* **2022**, *10*, 1–10, doi:10.1186/s40494-022-00743-0.
61. Wang, Z.; Su, S.; Ling, F.C.C.; Anwand, W.; Wagner, A. Thermal Evolution of Defects in Undoped Zinc Oxide Grown by Pulsed Laser Deposition. *J. Appl. Phys.* **2014**, *116*, doi:10.1063/1.4890460.
62. Smith, L.M.; Aitken, H.M.; Coote, M.L. The Fate of the Peroxyl Radical in Autoxidation: How Does Polymer Degradation Really Occur? *Acc. Chem. Res.* **2018**, *51*, 2006–2013, doi:10.1021/acs.accounts.8b00250.
63. Hossain, F.M.; Murch, G.E.; Belova, I. V.; Turner, B.D. Electronic, Optical and Bonding Properties of CaCO3 Calcite. *Solid State Commun.* **2009**, *149*, 1201–1203, doi:10.1016/j.ssc.2009.04.026.
64. Ishchenko, O.; Rogé, V.; Lamblin, G.; Lenoble, D.; Fechete, I. TiO2, ZnO, and SnO2-Based Metal Oxides for Photocatalytic Applications: Principles and Development. *Comptes Rendus Chim.* **2021**, *24*, 103–124, doi:10.5802/CRCHIM.64.
65. Lipovsky, A.; Tzitrinovich, Z.; Friedmann, H.; Applerot, G.; Gedanken, A.; Lubart, R. EPR Study of Visible Light-Induced Ros Generation by Nanoparticles of ZnO. *J. Phys. Chem. C* **2009**, *113*, 15997–16001, doi:10.1021/jp904864g.
66. Kraeutler, B.; Jaeger, C.D.; Bard, A.J. Direct Observation of Radical Intermediates in the Photo Kolbe Reaction—HeterogeneousPhotocatalytic Radical Formation by Electron Spin Resonance. *J. Am. Chem. Soc.* **1978**, *100*, 4903–4905, doi:10.1021/ja00483a052.
67. Schmitt, M. ZnO Nanoparticle Induced Photo-Kolbe Reaction, Fragment Stabilization and Effect on Photopolymerization Monitored by Raman-UV-Vis Measurements. *Macromol. Chem. Phys.* **2012**, *213*, 1953–1962, doi:10.1002/macp.201200309.
68. Ibraheem, H.A.; El-Hiti, G.A.; Yousif, E.; Ahmed, D.S.; Hashim, H.; Kariuki, B.M. Investigation of the Impact of Chemical Modifications on the Photostability of Polymethyl Methacrylate. *Int. J. Polym. Sci.* **2024**, *2024*, doi:10.1155/2024/3354280.
69. Sansul, S.; Yousif, E.; Ahmed, D.S.; El-Hiti, G.A.; Kariuki, B.M.; Hashim, H.; Ahmed, A. Pendant Modification of Poly(Methyl Methacrylate) to Enhance Its Stability against Photoirradiation. *Polymers (Basel).* **2023**, *15*, 1–15, doi:10.3390/polym15142989.
70. Kaczmarek, H.; Szalla, A. Photochemical Transformation in Poly(Acrylic Acid)/Poly(Ethylene Oxide) Complexes. *J. Photochem. Photobiol. A Chem.* **2006**, *180*, 46–53, doi:10.1016/j.jphotochem.2005.09.014.